frontiers in Materials

ORIGINAL RESEARCH
published: 12 February 2021
doi: 10.3389/fmats.2021.633789

Influence of Coarse Mg_3Bi_2 Particles on Deformation Behaviors of Mg-Bi Alloys

Tingting Guo[1†], Xuerong Lu[1†], Ramesh Kumar Varma[2], Cheng Zhao[3], Jun Wang[2], Jianwei You[1] and Jian Chen[1]*

[1]School of Materials Science and Chemical Engineering, Xi'an Technological University, Xi'an, China, [2]Institute for Frontier Materials, Deakin University, Geelong, VIC, Australia, [3]School of Materials Science and Engineering, Xi'an University of Technology, Xi'an, China

Mg-Bi binary alloys with concentrations of 1, 3, 6, and 9 wt% Bi and ternary Mg-9Bi-2.5Zn alloy were prepared by casting and hot extrusion. The results show that alloying with Bi refined as-cast grains of Mg alloys and the refinement efficiency of Bi is in between Al and Zr. It was also found that a critical value for the area fraction of constituent Mg_3Bi_2 particles seems to appear, which influences the dynamic recrystallization mechanism during extrusion. This influence results in either uniform or heterogenetic distribution of grain size and different extrusion texture intensities. Furthermore, the addition of Zn affected both the grain size and the area fraction/size of Mg_3Bi_2. Mechanical results and microstructure/fractography observation suggest that Mg_3Bi_2 particles do not impact the tensile nor compression yielding stress but act as fracture sources.

Keywords: magnesium, bismuth, zinc, coarse particles, deformation behavior

OPEN ACCESS

Edited by:
Minghui Cai,
Northeastern University, China

Reviewed by:
Hucheng Pan,
Northeastern University, China
Zhen Zhang,
Hefei University of Technology, China

****Correspondence:***
Tingting Guo
ttgu@outlook.com

†These authors have contributed equally to this work

Specialty section:
This article was submitted to Structural Materials, a section of the journal Frontiers in Materials

Received: *26 November 2020*
Accepted: *04 January 2021*
Published: *12 February 2021*

Citation:
Guo T, Lu X, Varma RK, Zhao C, Wang J, You J and Chen J (2021) Influence of Coarse Mg_3Bi_2 Particles on Deformation Behaviors of Mg-Bi Alloys. Front. Mater. 8:633789. doi: 10.3389/fmats.2021.633789

INTRODUCTION

Alloying is a common manner to modify the microstructure and the mechanical response of magnesium (Mg). Zinc (Zn), aluminum (Al), and rare earth (RE) are the main alloying elements for commercial applications of Mg alloys at present (Ahmad et al., 2019; Jayasathyakawin et al., 2020; Polmear et al., 2017c). With alloying and subsequent metallurgical/thermal treatments, intermetallic compounds, submicron-sized particles, or nanosized precipitations are usually formed in these magnesium alloys. These particles usually exert diverse influences on plastic deformation behaviors of the end products. A better understanding of the role played by them in the mechanical properties of Mg alloys is thereby essential for designing sophisticated new alloys.

Fine and densely dispersed particles are ideal for alloys to obtain a well-balanced strength and ductility. Efforts have been made to work on age-hardenable magnesium to achieve this goal for decades and an Mg-Bi system in recent years has attracted increasing attention due to its great mechanical properties (Go et al., 2020; Meng et al., 2020). Nanosized Mg_3Bi_2 precipitates are usually formed during the age heat treatment of Mg-Bi alloys and they show rod- or plate-like shapes lying parallel to $\langle 11\bar{2}0\rangle$ or $\langle 10\bar{1}0\rangle$ directions of Mg matrix (Sasaki et al., 2009; Sun and Sun, 2018). Zn coworks with bismuth (Bi) in Mg to further refine the Mg_3Bi_2 precipitates by around two- to fivefold while promoting the nucleation of Mg_3Bi_2 (Sasaki et al., 2009; He et al., 2020). Nanosized Mg_3Bi_2 particles could be obtained during the postthermal processing and the area fraction is in a positive linear relationship with Bi addition (Yu et al., 2020). The binary or multicomponent Mg-Bi-based alloys containing very fine precipitations were reported to show an improved hardening response (Sasaki et al., 2009; He et al., 2020). On the other hand, the constituent Mg_3Bi_2 phase formed during

TABLE 1 | Composition of the alloys studied in this work expressed in weight percentage.

Alloy	Bi	Zn	Mg
Mg-1Bi	1.05	—	Balance
Mg-3Bi	3.08	—	Balance
Mg-6Bi	5.69	—	Balance
Mg-9Bi	8.67	—	Balance
Mg-9Bi-2.5Zn	9.26	2.54	Balance

solidification cannot dissolve comprehensively in homogenization, due to its high incipient melting temperature (Go et al., 2020). This constituent Mg_3Bi_2 phase is expected to impose a different effect on mechanical performance compared to the same phase with much smaller sizes obtained by postthermal processing. However, this effect is not well understood.

Meng et al. (Meng et al., 2017) observed that stringers of coarse Mg_3Bi_2 intermetallic compounds, with an area fraction of ~5.9%, were aligned along the extrusion direction (ED) in an Mg-8Bi-1Al-1Zn alloy. This extruded alloy showed a yield stress of ~291 MPa with an elongation of ~14.6%. These good mechanical properties were ascribed to the refined grain size and the hardening effect by Mg_3Bi_2. In another investigation on Mg-6Bi and Mg-9Bi alloys (Go et al., 2020), the tensile yield stress was measured as ~129 MPa and 141 MPa, respectively, and both materials showed brittle fracture (~5% elongation). The stress increment was interpreted as a change of the coarse Mg_3Bi_2 particles' area fraction from 12.7% to 14.4%. In a very recent work by Yu et al. (Yu et al., 2020), the influence of 2, 5, and 8 wt% bismuth addition on the microstructure and plastic deformation of binary magnesium alloys was examined. Their results showed that the yielding systematically rises with Bi content, and the Mg-5Bi had the best ductility of ~19.8%. Both nanosized precipitates and coarse phase of Mg_3Bi_2 were observed and explained to contribute to the hardening. The crack types of either brittle or ductile fracture mentioned above were caused by the large Mg_3Bi_2 compounds judging from the fractography. However, the microstructure features, i.e., the size of these Mg_3Bi_2 particles, whether they are nanosized or coarse or a mixture of both, on the mechanical performance, were not well separated. It is expected that the size of these particles should play an important role. Therefore, the present study focuses on examining the effect of coarse Mg_3Bi_2 particles.

Specifically, in this work, binary Mg-Bi alloys with 1, 3, 6, and 9 wt% addition were employed for investigation. We aim at studying the role of coarse Mg_3Bi_2 particles obtained from the casting on plastic deformation, and the influence of Zn will also be discussed.

EXPERIMENTAL METHOD

Five alloys listed in **Table 1** were studied in this work, and pure Mg was used for the benchmark. The castings were heated to 730°C and then poured into a 300°C preheated brass mold to produce an as-cast cylinder of 85 mm in diameter and 200 mm in length. The compositions of all alloys were analyzed during the casting by Inductively Coupled Plasma (ICP) Spectroscopy to obtain the targeting compositions. The as-cast ingots were homogenized at 500°C for 24 h and then machined to a diameter of ϕ80 mm. The ingots were extruded at 380°C with an extrusion ratio of 25 : 1 at a ram speed of 2 m/min and finished with water quenching. Dog-bone shaped tensile samples with a gauge dimension of ϕ3 mm × 10 mm and cylindrical compression specimens with the size of ϕ10 mm × 15 mm were prepared. The ambient temperature tensile and compression tests were performed at a strain rate of 10^{-3}/s. The tensile strain is measured by a contact extensometer (Epsilon, produced by Epsilon Technology Corp, USA) until fracture.

The samples for Optical Microscopy (OM), Scanning Electron Microscopy (SEM), Energy-Dispersive X-ray (EDX) spectroscopy, and Electron Backscattered Diffraction (EBSD) observations were taken close to the cylindrical axis and polished on the cross-sectional surface of the casting or extrusion parts. The polishing procedure includes wet grinding using 2000 grit SiC paper and 6 and 3 μm diamond pastes. The 20 nm sized colloidal silica was used for the last step on a Struers DP-Pan cloth. Samples were ultrasonically cleaned for 2 min in ethanol between each step and dried with flowing air. The samples for OM observations were etched in acetic-nitric acid (15 ml acetic acid, 5 ml nitric acid, 60 ml ethanol, and 20 ml distilled water) for 5–10 s depending on the content of Bi. SEM and EDX analyses were performed using a VEGA3-SBH Tescan operated at 20 kV. ImageJ software (Schneider et al., 2012) was used for particle analysis. The textures obtained by EBSD mapping were carried out by a field emission Zeiss Sigma 500 and the scanning step size is 1–3 μm decided by the grain size of samples. An HKL channel five software (Oxford Instruments) was employed for EBSD analysis. Phase determination was performed on 2000 grid SiC polished surface using Bruker D2 Phaser X-Ray Diffractometer (XRD) by Cu Kα radiation. The lattice parameters were calculated by single peak refinement from the corrected peak positions [Suryanarayana and Norton, 1998]. A nonlinear least-square refinement over the observed *hkl* reflections and the corresponding *d* spacing gives lattice parameters.

RESULTS

Microstructure of As-Cast Alloys

Figure 1 shows the as-cast microstructures of alloys investigated in the present work. There is interdendritic segregation that occurs in the alloys with higher bismuth concentration (**Figures 1D,E**). Smaller dendritic arms were observed in ternary alloys due to the influence of Zn, shown in **Figure 1F**, and some large particles were also seen in the grain interior. Taking a close inspection of Mg-9Bi (**Figure 2A**) and Mg-9Bi-2.5Zn (**Figure 2B**), most of the intermetallic compounds lie along the grain boundaries, and there are rod-like submicron-sized particles located around. EDX results show that the intermetallic compounds and the submicron-sized particles are composed of

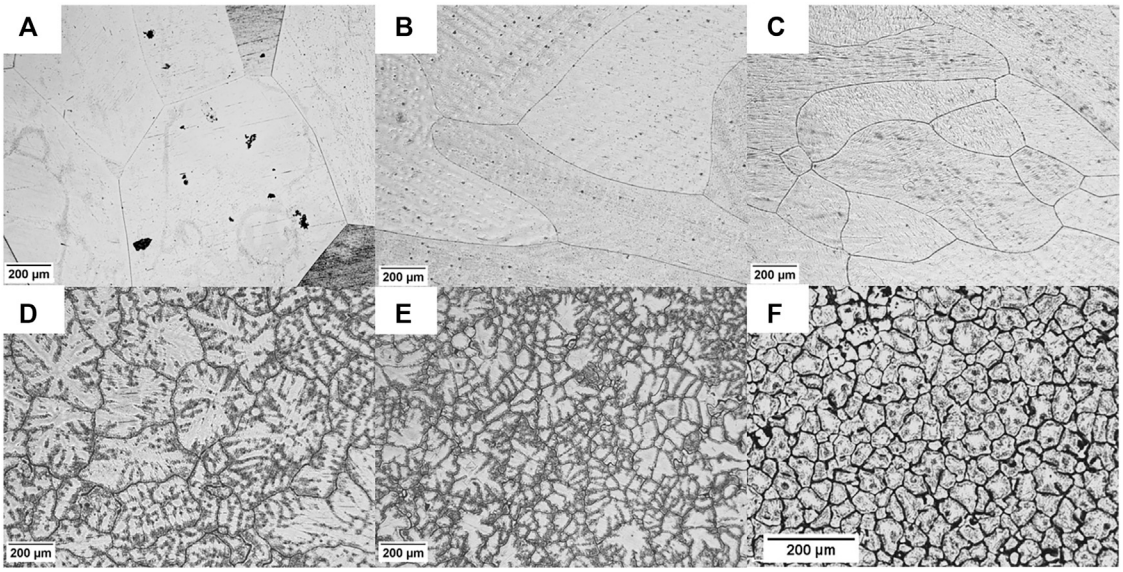

FIGURE 1 | As-cast microstructure of **(A)** pure Mg, **(B)** Mg-1Bi, **(C)** Mg-3Bi, **(D)** Mg-6Bi, **(E)** Mg-9Bi, and **(F)** Mg-9Bi-2.5Zn.

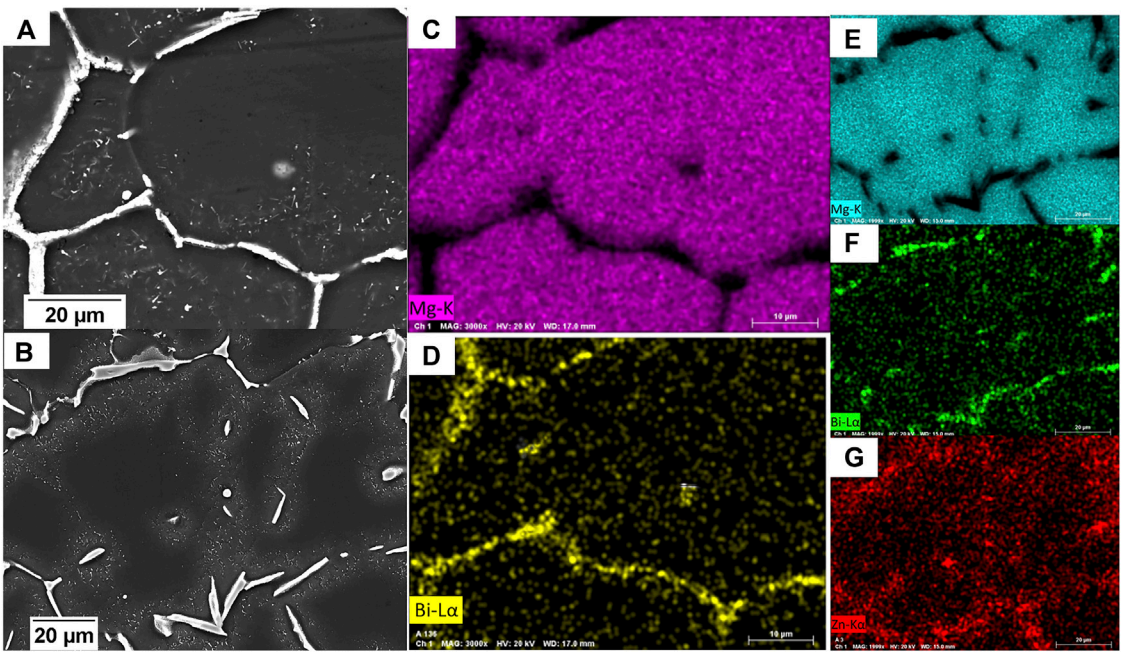

FIGURE 2 | EDX analysis of **(A) (C) (D)** Mg-9Bi alloy and **(B) (E) (F) (G)** Mg-9Bi-2.5Zn.

Mg_3Bi_2 phase, which has been further confirmed by XRD analysis (not shown here). The rod-shaped particles' size is estimated to be ~1.5 times smaller in ternary alloys than that in Mg-9Bi. It was shown in **Figure 2** that the Bi is rarely concentrated in the grain interior, indicative of the serious segregation feature of the Bi element. There is a segregation-free and precipitation-free zone adjacent to the coarse intermetallic compounds/grain boundaries, which is not uncommon in aged alloys (Watanabe et al., 2008; Zindal et al., 2018).

Figure 3A depicts the evolution of grain size with compositions. Bi acts as a grain refiner and reduces the average grain size from 880 μm of pure Mg to 115 μm when 9 wt% Bi is added. The grain size is further reduced to 47 μm by alloying with Zn. **Figure 3B** shows the statistics of area fraction of

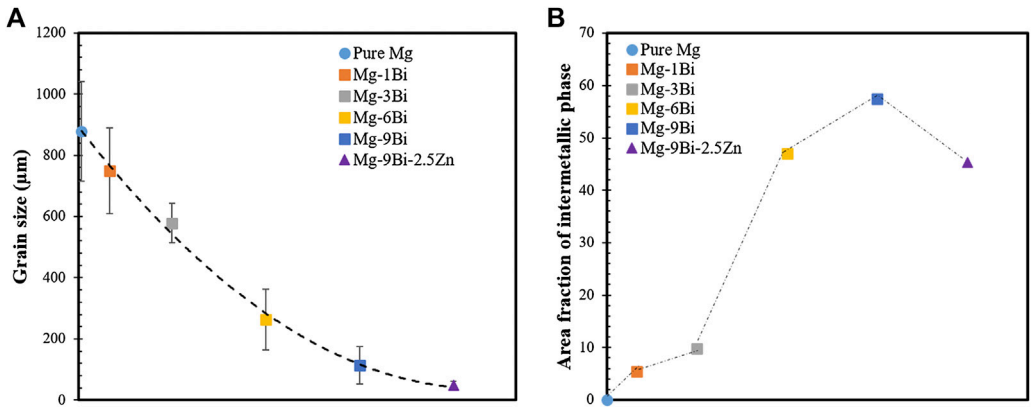

FIGURE 3 | (A) The evolution of grain size with Bi content and **(B)** the area fraction of Mg_3Bi_2 intermetallic compounds of alloys estimated by ImageJ. The error bars represent the standard deviation. The dashed line is used for guiding the eyes.

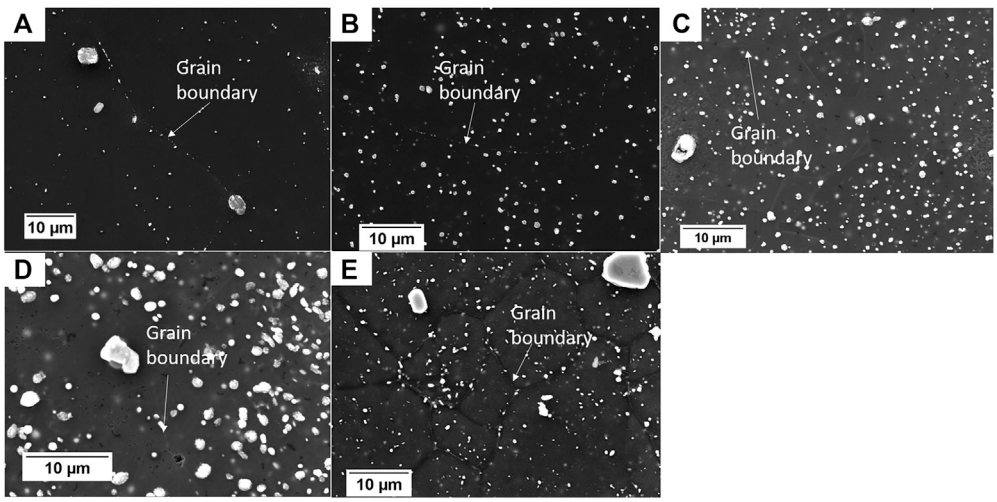

FIGURE 4 | SEM images showing microstructure of extruded **(A)** Mg-1Bi, **(B)** Mg-3Bi, **(C)** Mg-6Bi, **(D)** Mg-9Bi, and **(E)** Mg-9Bi-2.5Zn.

intermetallic phase along the grain boundaries. ImageJ was employed on OM images to analyze based on the contrast with Mg matrix. This method overestimates the amount of Mg_3Bi_2, because the area of Bi segregation is not easy to be excluded, and it are only used for rough comparison. It is observed that the amount of Mg_3Bi_2 phase (and Bi segregation) increases with Bi content and reaches a peak of 57% area fraction for the Mg-9Bi alloy. Further alloying with Zn, by contrast, decreases the Mg_3Bi_2 area fraction, which is even 1.7% less than that for the Mg-6Bi.

Microstructure and Texture of Extruded Alloys

Figure 4 shows the SEM images of the cross-sectional plane of the extruded alloys. The XRD profiles in **Figure 5** index the Mg_3Bi_2 particles in all alloys. Mg_3Bi_2 particles are observed on both grain boundaries and interiors. The average diameter of particles is shown to be the largest in Mg-9Bi of ~0.65 μm, although the data is widely scattered, as observed in **Figure 6A**. In contrast, the other alloys display a similar average size of ~0.4 μm. The area fraction of particles in **Figure 6B** follows the same trend as observed in **Figure 3B**. The values shown in **Figure 6B** drop sharply below 10%, which is possible due to the dissolution of the segregated Bi. Alloy of 9% Bi contains the largest area fraction of the second phase of ~7.3%, while only ~5.7% Mg_3Bi_2 particles are present in the ternary alloy.

Figure 5 shows XRD profiles of Mg-Bi and Mg-Bi-Zn alloys. The primary Mg phase and secondary Mg_3Bi_2 phase are readily indexed. It can be seen that the intensity of Mg_3Bi_2 phase increases with Bi concentration. However, due to the orientation effect in the irradiated area, the peak intensities do not follow the reference intensity ratio (RIR) values. Further, the

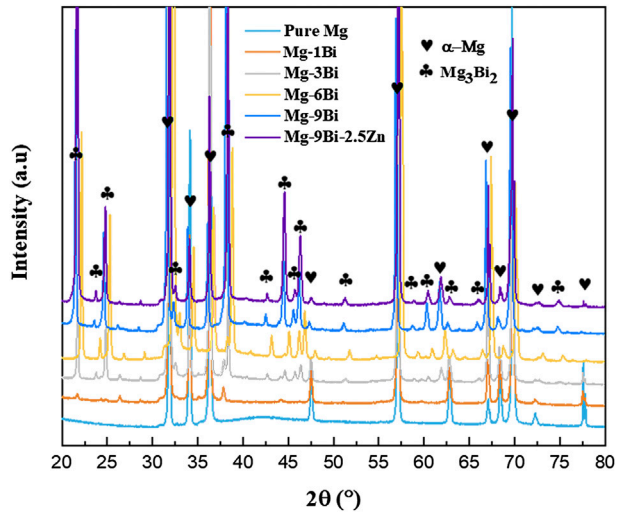

FIGURE 5 | XRD profiles of pure Mg, Mg-Bi, and Mg-Bi-Zn alloys.

effect of Bi on Mg matrix will be analyzed via lattice parameter variation in the discussion section.

The microstructures of the as-extruded materials and their corresponding inverse pole figure (IPF) are shown in **Figures 7** and **8**, respectively. The grains are dramatically refined (see caption of **Figure 7** for more details) compared to the as-cast counterpart. The heterogeneity of grain size in Mg-6Bi and Mg-9Bi indicates the partially dynamic recrystallized (DRXed) microstructure, which accounts for 38.8% and 89.4% in area fraction, respectively. The formation of DRXed grains in those two alloys might be due to a precipitation stimulated nucleation (PSN) mechanisms by the presence of isolated large Mg_3Bi_2 particles. It is generally accepted that PSN is observed to occur at particles with a diameter larger than 1 μm (Robson et al., 2009; Doherty et al., 1997; Humphreys et al., 2017), which accounts for ~4%, ~3.5%, ~7%, and ~19% of total particles in binary alloys with an increase of Bi content, and in Mg-9Bi-2.5Zn alloys, it is ~6%. The efficiency of PSN seems to be influenced by fraction of critical-sized (1 μm) particles, and a value of ~7% might be the threshold based on the dynamic recrystallization fraction changes. It is worth noting that the PSN-induced DRXed grains in the Mg-6Bi and Mg-9Bi alloys display the strongest $[10\bar{1}0]$ fiber texture (~5.5 MUD, analyzed by partition DRXed grains according to kernel average misorientation). Inspection of the grain disorientation function in **Figure 9** reveals that all the materials have experienced recrystallization (>90% grain boundaries are high angle ones). The less intense texture (**Figures 8A–C,F**) and homogeneously distributed grain size in other alloys imply possible different DRXed mechanisms rather than PSN. For particle size smaller than the critical value, the recrystallization could be retarded resulting in an increase of grain size (Humphreys et al., 2017), which probably occurred in the current alloys Mg-1Bi, Mg-3Bi, and Mg-9Bi-2.5Zn. A careful examination of Mg_3Bi_2 particle-stimulated dynamic recrystallization will be presented in a separate paper.

Mechanical Properties

Engineering stress-strain curves obtained from tensile and compression tests for pure Mg and magnesium alloys are presented in **Figures 10A** and **10B**. The effect of alloying with Bi and Zn on the 0.2% offset yield strength is summarized in **Figure 10C**. Tensile yield stress increases with the Bi concentration up to 6%. A drop of yielding of ~26 and ~29 MPa can be observed when going from the addition of 6%–9% of Bi to 9% Bi-2.5% Zn, respectively. Mg-9Bi-2.5Zn shows the best ductility with total elongation of ~10%, which is 3 times better than that for Mg-9Bi alloy. All the other alloys are brittle with the elongation of less than 5%. In the case of compression testing, the drop of yielding stress occurs in Mg-9Bi-2.5Zn by 14 MPa compared to Mg-9Bi. It is clear that the Bi addition is favorable for dampening yield asymmetry and the final addition of 2.5% Zn to Mg-9Bi alloy makes the asymmetry ratio (compression yield stress/tensile yield stress) close to 1, as shown in **Figure 10D**.

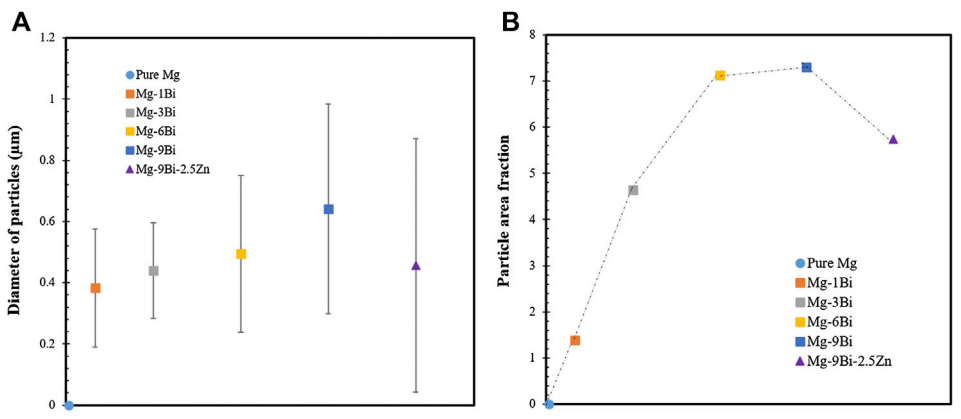

FIGURE 6 | (A) Diameter and **(B)** area fraction of Mg_3Bi_2 particles in pure Mg and alloys studied in the present work. ImageJ is used for analysis based on SEM images. The error bars represent the standard deviation. The dashed line is used for guiding the eyes.

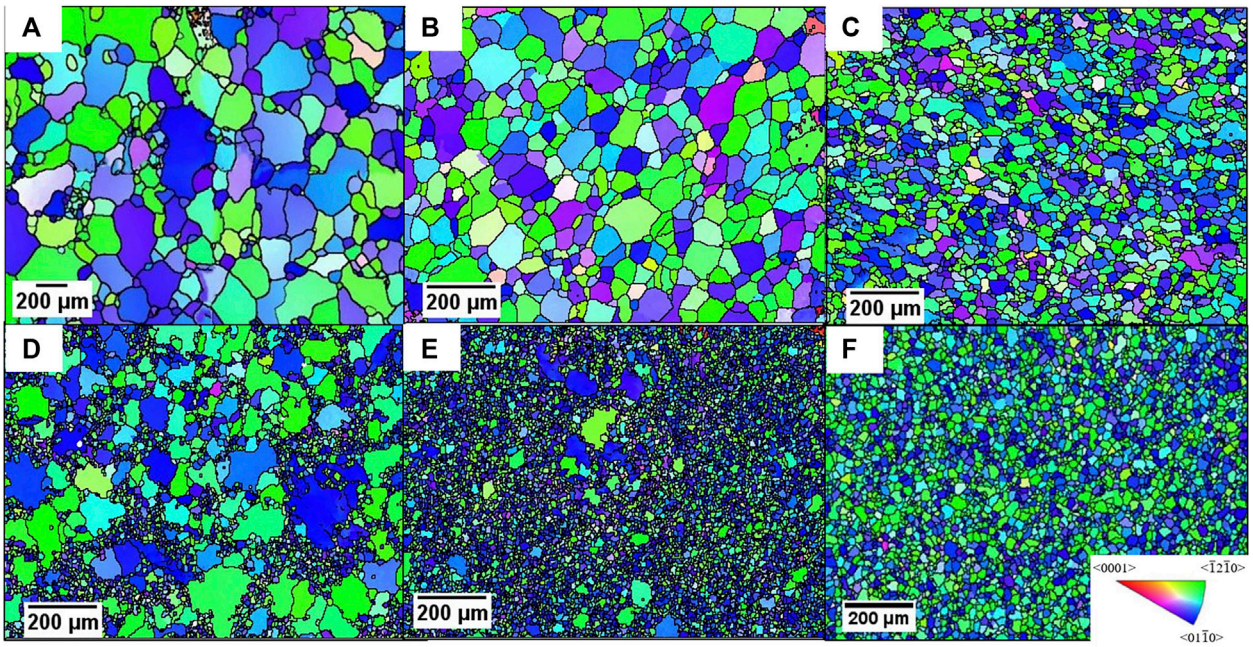

FIGURE 7 | Inverse pole figure colored EBSD maps of **(A)** pure Mg, **(B)** Mg-1Bi, **(C)** Mg-3Bi, **(D)** Mg-6Bi, **(E)** Mg-9Bi, and **(F)** Mg-9Bi-2.5Zn. The average grain size is 103, 38, 21, 15, 9, and 12 μm, respectively. The extrusion direction (ED) is normal to the page. The scanning area is in the center of the cross section of extrusion bars.

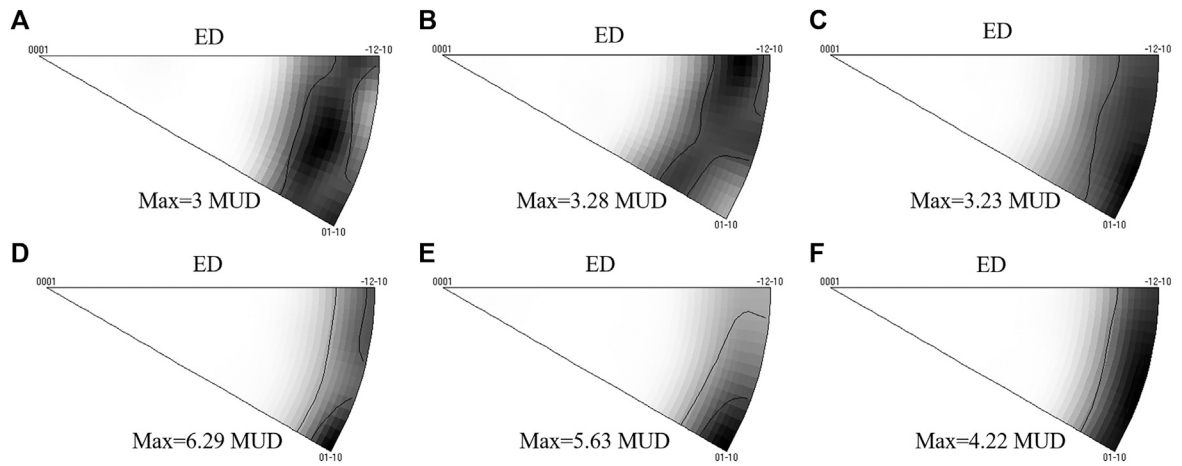

FIGURE 8 | Inverse pole figures of **(A)** pure Mg, **(B)** Mg-1Bi, **(C)** Mg-3Bi, **(D)** Mg-6Bi, **(E)** Mg-9Bi, and **(F)** Mg-9Bi-2.5Zn.

The fracture surface after tensile testing is shown in **Figure 11**. The typical brittle fracture featured with the cleavage plane is observed in pure Mg and Mg-1Bi. Both dimple-like failure and low ductility cleavage plane are observed in Mg-3Bi, Mg-6Bi, and Mg-9Bi. The Mg-9Bi-2.5Zn alloy demonstrates an almost uniform fracture consisting of dimples and river-like strips. Mg_3Bi_2 particles can be clearly seen inside the dimples in most alloys, except pure Mg and Mg-1Bi, indicating that these particles are probably the source of fracture. The average size of exposed particles is estimated to be ~0.27, 0.54, 0.62, and 0.34 μm for Mg-3Bi, Mg-6Bi, Mg-9Bi, and Mg-9Bi-2.5Zn, respectively, falling in the range of measurement shown in **Figure 6A**.

DISCUSSION

Grain Refinement of As-Cast Mg-Bi Alloys

Obtaining a fine-grained structure of as-cast alloys could reduce the need for postthermal processing or further refining the DRXed grains. As observed in **Figure 1**, alloying with Bi is a

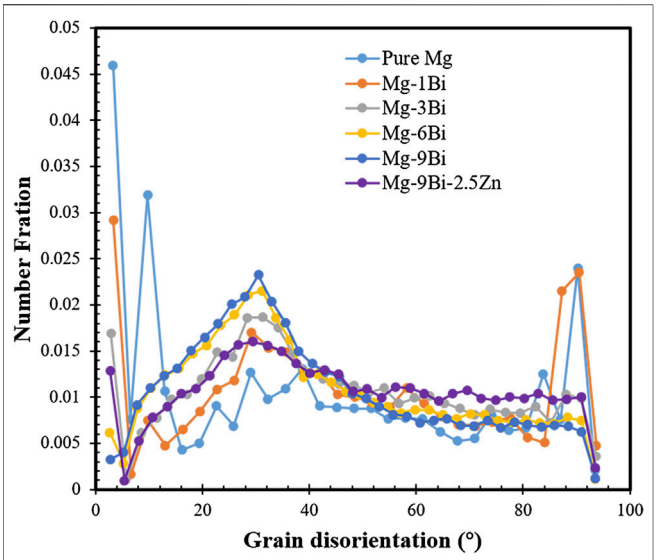

FIGURE 9 | Grain disorientation profile of as-extruded pure Mg and alloys studied in the present work.

potential option for grain refiner of magnesium alloys. The grain size is thought to be controlled by nucleant particles and growth restriction, Q. The solute with a strong segregation ability has a high Q value. The independence model incorporated two factors to predict the grain size, and the simplified version is (StJohn et al., 2013)

$$d = \frac{5.6Dz\Delta T_n}{v}\frac{1}{Q} + x_{sd}, \quad (1)$$

where D is the diffusion rate, z is the proportion of constitutional supercooling (CS) required to be regenerated after the nucleation, $1/\Delta T_n$ is the nucleant particle potency, v is the steady-state growth rate, and x_{sd} is the density of the particle. The growth restriction factor Q can be expressed as (Easton et al., 2016)

$$Q = C_0 m_1 (k - 1), \quad (2)$$

where C_0 is alloy composition, m_1 is the slope of the liquidus line, and k is the partition coefficient. The first term in **Eq. 1** is the distance of Nucleation Free Zone (NFZ), x_{nfz}, which is controlled by CS. Reducing the NFZ is the key to refine the grain size and the importance has been discussed in ref. (Easton et al., 2016; Prasad et al., 2013; StJohn et al., 2015). **Figure 12** plots the grain size against $1/Q$. The linear fitting equation though the data is d = 1194.5(1/Q) + 10. Joshi and Babu (Joshi and Hari Babu, 2017) studied the impact of 0.02 wt%–0.4 wt% Bi addition on the grain size of binary magnesium alloys and the relation of d_{gs} and $1/Q$ they obtained was d = 13.2(1/Q) + 403. Their result seems to show a greater grain refining effect by Bi. This is probably because the oxidation during casting which formed the Mg-Bi-O particles provides the nucleation sites in their work, while in our case, a

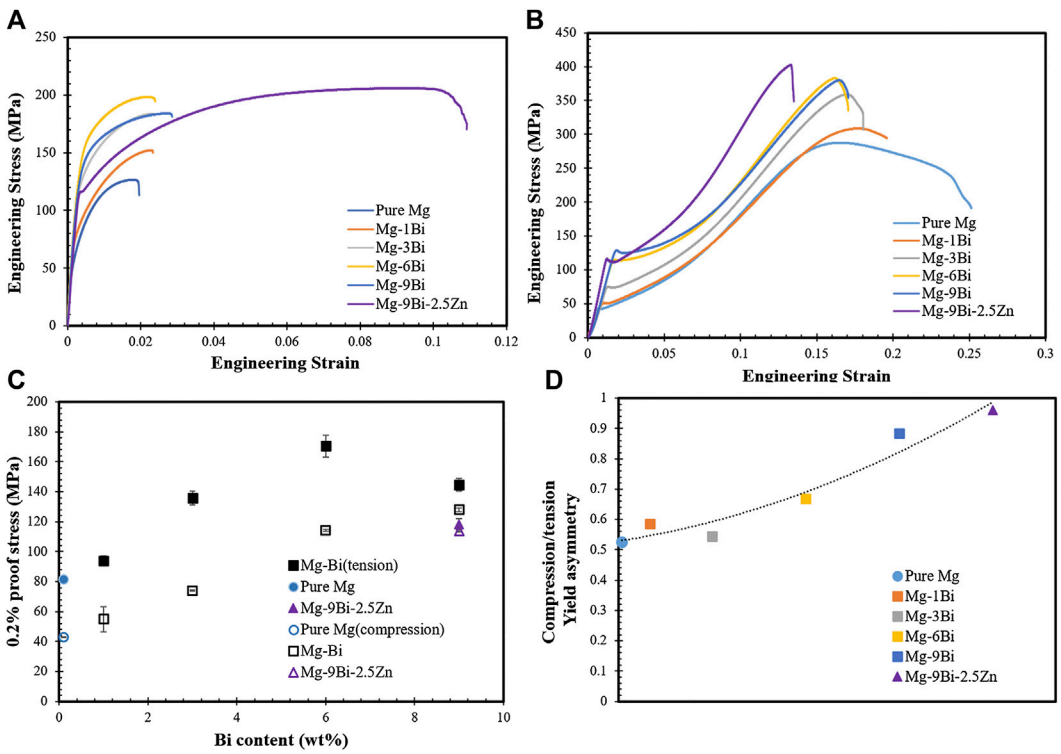

FIGURE 10 | Engineering stress-strain curve of **(A)** tensile, **(B)** compression tests, **(C)** summary of 0.2% offset proof stress, and **(D)** compression/tension yield asymmetry ratio in alloys studied in present work. The dashed line is used for guiding the eyes.

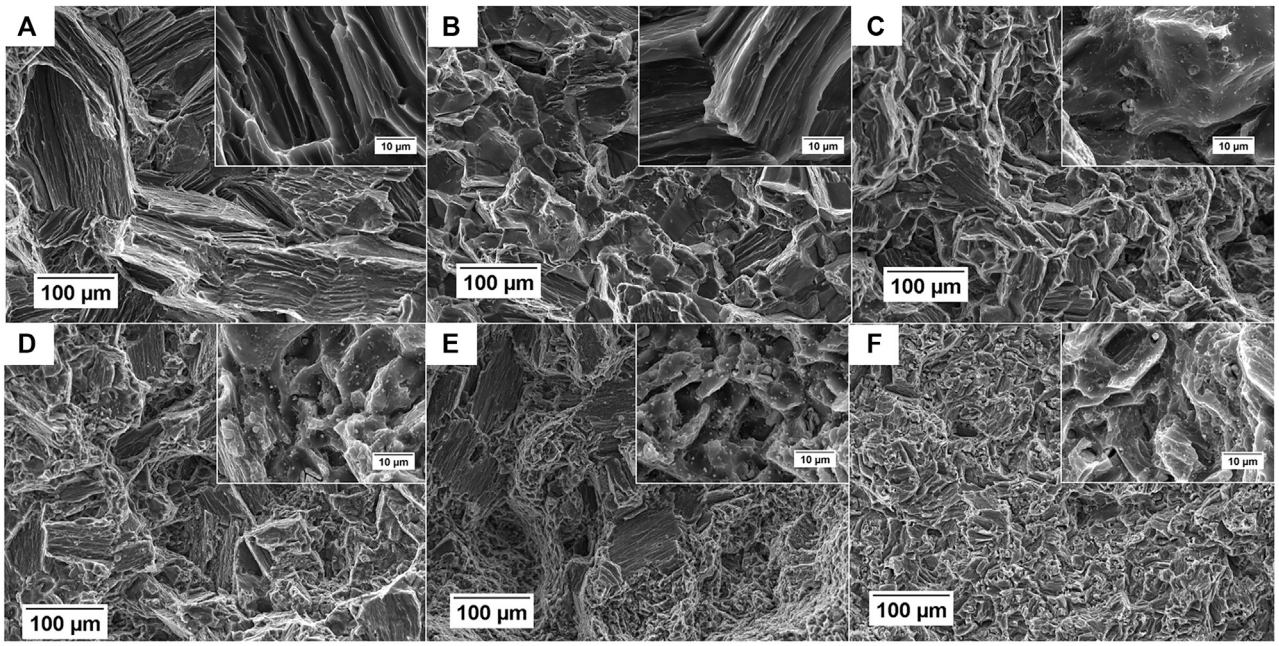

FIGURE 11 | Tensile fractograph of **(A)** pure Mg, **(B)** Mg-1Bi, **(C)** Mg-3Bi, **(D)** Mg-6Bi, **(E)** Mg-9Bi, and **(F)** Mg-9Bi-2.5Zn.

lower number of nucleating particles ($10/mm^3$) and large NFZ result in coarse grains. The data of Mg-Al and Mg-Zr cast in a mild steel mold reported by Lee et al. (Lee et al., 2000) are also plotted for comparison in **Figure 12**. If we neglect the effect of cooling rate (Bi is thought to be insensitive to the cooling rate by Joshi and Babu (Joshi and Babu, 2017)), the efficiency of Bi as a grain refiner for Mg is greater than Al but less than Zr. Zn is also thought to be a grain refiner to magnesium alloys (Polmear et al., 2017b) and leads to a further reduction of grain size when alloying with Zn.

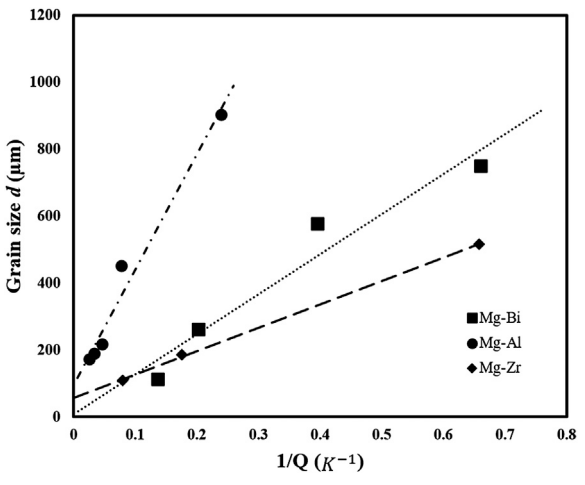

FIGURE 12 | Grain size vs. 1/*Q* for Mg-Bi (1-9 wt%) binary alloys. The casting was performed in a brass mold and the sample size is ϕ85 mm × L200 mm. The data of Mg-Al (1-9 wt%) and Mg-Zr (0.04-0.32 wt%) are reproduced from ref. Lee et al. (2000), and the sample dimension is ϕ25 mm × L70 mm.

The Variation of Yielding Stress

As observed in **Figure 10**, the tensile yielding stress increases with Bi addition in leaner alloys but drops at Mg-9Bi, and it has a further decrease in Mg-9Bi-2.5Zn alloy. The yield of compression rises as Bi concentration increases, and this is followed by a slight drop by 14 MPa alloyed with Zn. It seems that our work is controversial with previous reports (Yu et al., 2020; Go et al., 2020), in which the yielding monotonic increases with Bi content. The likely reasons will be analyzed in the following part.

As for textured extruded magnesium, tensile testing along the extrusion direction is controlled by prismatic slip, and for compression along the extrusion direction, the yielding is dominated by $\{10\bar{1}2\}$ extension twinning (Polmear et al., 2017c). The critical resolved shear stress (CRSS) for prismatic slip and extension twinning could thus be roughly estimated by multiplying the yielding stress (σ) and the average Schmid factor (M) as (Stanford and Barnett, 2013)

$$\mathrm{CRSS} = \sigma \Delta M. \tag{3}$$

Table 2 lists the CRSS of prismatic slip and twin for pure Mg and alloys, and the grain size is also presented for each extruded alloy. The CRSS values measured here are reasonable for both prismatic slip and extension twin for a range of grain sizes, which were reported by previous works (Ghaderi and Barnett, 2011; Stanford and Barnett, 2013). The grain size influences the activation of deformation modes; i.e., the smaller the grain size, the larger CRSS (Hall-Petch relation). This Hall-Petch type hardening is generally true for alloy up to 6 wt% Bi

TABLE 2 | Estimated critical resolved shear stresses for prismatic slip and extension twinning calculated from **Eq. 3**.

Material	*d* (μm)	$CRSS_{prism}$ (MPa)	$CRSS_{twin}$ (MPa)
Pure Mg	103	35.7	19
Mg-1Bi	38	40.5	23.6
Mg-3Bi	21	60.4	32.1
Mg-6Bi	15	77.7	48.1
Mg-9Bi	9	66.2	55.8
Mg-9Bi-2.5Zn	12	54.7	48.6

addition in our cases. It seems that alloying with 9% Bi softens the prismatic slip which is against this hardening law, and further alloying with 2.5% Zn softens both prismatic slip and extension twin.

Due to the consumption of Bi by a large amount of coarse Mg_3Bi_2 particles, we chose six different parts for each sample and carefully examined the Bi concentration that dissolved into the matrix as shown in **Figure 13A**. Zn is found to be ~2.5% in the matrix, which agrees with the ICP measurement. Note that the samples for ICP spectrometry are liquid so the Bi measured covers in both matrix and particles. Here, we focus on analyzing Mg-6Bi, Mg-9Bi, and Mg-9Bi-2.5Zn alloys because their grain sizes can be grouped into the same level. The concentration of Bi in Mg-6Bi matrix was measured the highest as ~4.8 wt% and was 3.5 wt% in Mg-9Bi and 1.84 wt% in Mg-9Bi-2.5Zn, respectively. The variations seem to follow the tendency of CRSS for the prismatic slip. It appears that the prismatic dislocations are more sensitive to Bi in solution than it is to the Mg_3Bi_2 particles. Besides, Stanford and Barnett (Stanford and Barnett, 2013) found the solute softening in binary Mg-Zn alloys because the stress for cross slip into the prismatic plane is lowered with higher solute content. It is believed that this is also a possible explanation for a further drop in the CRSS for prismatic slip in Mg-9Bi-2.5Zn. The coarse and brittle Mg_3Bi_2 particles could not effectively block the slip gliding but deteriorate the mechanical properties, e.g., ductility (**Figure 10A**). Similar findings were also seen in coarse particle-contained alloys (Gutierrez-Urrutia et al., 2005; Polmear et al., 2017a; Huang et al., 2018).

Figure 13B shows changes in the lattice parameter *a* "*a*" of the Mg phase, which can be calculated based on (Suryanarayana and Norton, 1998)

$$\frac{1}{d^2} = \frac{4}{3}\left(\frac{h^2 + hk + k^2}{a^2}\right) + \frac{l^2}{c^2}, \tag{4}$$

where *hkl* is the Miller indices, *a* and *c* are the lattice parameters, and *d* is the plane spacing. A systematic variation can be seen in the lattice parameter "*a*" with a dissolved solute concentration in the matrix in **Figure 13A**. The highest expansion was observed for the highest solution of Bi in the matrix. In contrast, a sharp contraction is observed upon the addition of Zn. These results are directly supportive of EDX measurement and can be understood via size effects. Bi is a slightly bigger atom than Mg. A gradual increase is observed in the lattice of Mg with an increase in Bi concentration. However, in the presence of Zn, a marked decrease in the lattice parameter is observed owing to the smaller atomic size of Zn. Similar behavior was reported in (Kennedy and Raynor, 1959). Therefore, we prefer to conclude that the hardening of the prismatic slip is dominated by solid solution strengthening mechanism and Hall-Petch type hardening. Mg_3Bi_2 particles have little impact on the observed yielding but cause a dramatic loss of ductility by acting as a brittle fracture source.

We turn now to the strengthening effect on twinning. Mg_3Bi_2 particles may provide sites for twin nucleation and possibly increase the twin number density, which is generally true in fine-precipitated magnesium alloys (Stanford and Barnett, 2009; Robson et al., 2010; Robson and Barnett, 2019; Jain et al., 2015). Based on the Orowan hardening law ($\Delta\tau \sim 1/\lambda \log(D_p/r_0)$, where λ is the interparticle spacing on twin plane, D_p is the diameter of particles, and r_0 is the dislocation core radius (Embury et al., 2016), the finer and close-spaced particles always show a good

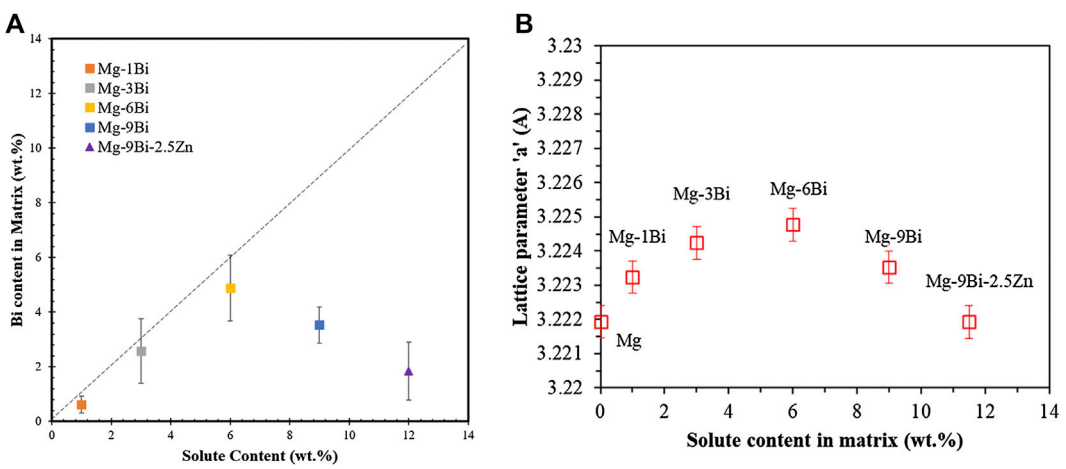

FIGURE 13 | (A) Bi concentration in matrix measured by EDX vs. Bi concentration obtained by ICP. The dashed line shows the idea case that Bi is dissolved thoroughly in the matrix. **(B)** Lattice parameter "*aa*" variation of Mg as a function of solute concentration in the matrix.

hardening against twinning. The overaged magnesium shows reduced hardening stress on twins compared with the peak-aged condition (Jain et al., 2015). As observed in **Figures 4** and **6A**, both the diameter and interparticle spacing are hundreds of times larger than the most effective fine precipitates generated during aging. It is less likely that the twin could be strengthened by the coarse Mg_3Bi_2 particles, at least on yielding. The hardening is more possibly caused by the reduced grain size in more heavily alloyed Mg, as shown in **Table 2**. It is not sure, to what extent, that the residual solute Bi left in the matrix plays a role in the hardening of twinning, which requires further examination.

CONCLUSION

In this study, a systematic investigation of the effect of Mg_3Bi_2 particles on deformation behavior in a series of Mg-Bi binary alloys and Mg-9Bi-2.5Zn was reported. The following are the conclusions drawn from this work:

1. The addition of Bi element to magnesium led to a reduction of grain size in casting. A linear expression of $d = 1194.5\,(1/Q) + 10$ was obtained. The grain refinement efficiency is greater than the addition of Al but less than Zr reported by Lee et al. (Lee et al., 2000).
2. The Mg_3Bi_2 particles could either stimulate or retard the dynamic recrystallization depending on the particle size and area fraction. The PSN DRXed grains show stronger $[10\bar{1}0]$ fiber texture intensity.
3. Coarse Mg_3Bi_2 particles cannot strengthen the prismatic slip nor the extension twin but cause ductility to lose. The tensile yielding dominated by prismatic slip is more sensitive to the Bi solute concentration. The compression yielding stress controlled by extension twin activation is influenced by Hall-Petch type strengthening. Mg_3Bi_2 particles serve as fracture source in the tensile testing.
4. The addition of Zn can refine the Mg-Bi casting microstructure and reduce the size and area fraction of Mg_3Bi_2 particles.

DATA AVAILABILITY STATEMENT

The original contributions presented in the study are included in the article/Supplementary Material; further inquiries can be directed to the corresponding author.

AUTHOR CONTRIBUTIONS

TG designed the experiments and wrote the manuscript. XL performed the experimental work of binary alloys and analyzed data. RK calculated the lattice parameter and revised the manuscript. CZ performed the experimental work of ternary alloy. JW designed the experiments and revised the manuscript. JY performed the XRD measurement. JC revised the manuscript.

FUNDING

The authors are grateful for the financial support from the National Natural Science Foundation of China (NSF) (Grant No. 51901169) and the Special Scientific Research Program of Shaanxi Provincial Department of Education (No. 2019-112-01). The authors would also like to thank the Yinguang Magnesium Industry Group for the provision of materials. Weihai Langu Institute for Material Analysis is also appreciated for providing advanced microscope.

REFERENCES

Ahmad, R., Yin, B., Wu, Z., and Curtin, W. A. (2019). Designing high ductility in magnesium alloys. *Acta Mater.* 172, 161–184. doi:10.1016/j.actamat.2019.04.019

Doherty, R. D., Hughes, D. A., Humphreys, F. J., Jonas, J. J., Jensen, D. J., Kassner, M. E., et al. (1997). Current issues in recrystallization: a review. *Mater. Sci. Eng. A.* 238 (2), 219–274. doi:10.1016/S0921-5093(97)00424-3

Easton, M. A., Qian, M., Prasad, A., and St John, D. H. (2016). Recent advances in grain refinement of light metals and alloys. *Curr. Opin. Solid State Mater. Sci.* 20 (1), 13–24. doi:10.1016/j.cossms.2015.10.001

Embury, J. D., Lloyd, D. J., and Ramachandran, T. R. (2016). "22 - strengthening mechanisms in aluminum alloys," in *Treatise on materials science and Technology*. Editors A. K. Vasudevan and R. D. Doherty Amsterdam, Netherlands: Elsevier, 579–601.

Ghaderi, A., and Barnett, M. R. (2011). Sensitivity of deformation twinning to grain size in titanium and magnesium. *Acta Mater.* 59 (20), 7824–7839. doi:10.1016/j.actamat.2011.09.018

Go, J., Jin, S.-C., Kim, H., Yu, H., and Park, S. H. (2020). Novel Mg–Bi–Al alloy with extraordinary extrudability and high strength. *J. Alloys Compd.* 843, 156026. doi:10.1016/j.jallcom.2020.156026

Go, J., Lee, J. U., Yu, H., and Park, S. H. (2020). Influence of Bi addition on dynamic recrystallization and precipitation behaviors during hot extrusion of pure Mg. *J. Mater. Sci. Technol.* 44, 62–75. doi:10.1016/j.jmst.2019.10.036

Gutierrez-Urrutia, I., Muñoz-Morris, M. A., and Morris, D. G. (2005). The effect of coarse second-phase particles and fine precipitates on microstructure refinement and mechanical properties of severely deformed Al alloy. *Mater. Sci. Eng. A.* 394 (1), 399–410. doi:10.1016/j.msea.2004.11.025

He, C., Liu, C. Q., Chen, H. W., and Nie, J. F. (2020). Enhanced age-hardening response in Mg–Zn–Co alloys with Bi additions. *J. Alloys Compd.* 815, 152419. doi:10.1016/j.jallcom.2019.152419

Huang, K., Marthinsen, K., Zhao, Q., and Logé, R. E. (2018). The double-edge effect of second-phase particles on the recrystallization behaviour and associated mechanical properties of metallic materials. *Prog. Mater. Sci.* 92, 284–359. doi:10.1016/j.pmatsci.2017.10.004

Humphreys, J., Rohrer, G. S., and Rollett, A. (2017). "Chapter 9 - recrystallization of two-phase Alloys," in *Recrystallization and related annealing phenomena*. 3rd Edn (Oxford, United Kingdom: Elsevier), 321–359.

Jain, J., Cizek, P., Poole, W. J., and Barnett, M. R. (2015). The role of back stress caused by precipitates on $\{101^{-}2\}$ twinning in a Mg–6Zn alloy. *Mater. Sci. Eng. A.* 647, 66–73. doi:10.1016/j.msea.2015.08.091

Jayasathyakawin, S., Ravichandran, M., Baskar, N., Anand Chairman, C., and Balasundaram, R. (2020). Mechanical properties and applications of Magnesium alloy – Review. *Mater. Today Proc.* 27, 909–913. doi:10.1016/j.matpr.2020.01.255

Joshi, U., and Hari Babu, N. (2017). The grain refinement potency of bismuth in magnesium. *J. Alloys Compd.* 695, 971–975. doi:10.1016/j.jallcom.2016.10.215

Kennedy, A. J., and Raynor, G. V. (1959). *The physical metallurgy of magnesium and its alloys*. London, United Kingdom: Pergamon Press, 531.

Lee, Y. C., Dahle, A. K., and Stjohn, D. H. (2000). The role of solute in grain refinement of magnesium. *Metall. Mater. Trans.* 31 (11), 2895–2906. doi:10.1007/BF02830349

Meng, S. J., Yu, H., Fan, S. D., Kim, Y. M., Park, S. H., Zhao, W. M., et al. (2020). A high-ductility extruded Mg-Bi-Ca alloy. *Mater. Lett.* 261, 127066. doi:10.1016/j.matlet.2019.127066

Meng, S., Yu, H., Zhang, H., Cui, H., Park, S. H., Zhao, W., et al. (2017). Microstructure and mechanical properties of an extruded Mg-8Bi-1Al-1Zn (wt%) alloy. *Mater. Sci. Eng. A*. 690, 80–87. doi:10.1016/j.msea.2017.02.095

Polmear, I., StJohn, D., Nie, J.-F., and Qian, M. (2017a). "2 - physical metallurgy of aluminium alloys," in *Light alloys*. 5th Edn (Boston, MA: Butterworth-Heinemann), 31–107.

Polmear, I., StJohn, D., Nie, J.-F., and Qian, M. (2017b). "3 - casting of light alloys," in *Light alloys*. 5th Edn (Boston: Butterworth-Heinemann), 109–156.

Polmear, I., StJohn, D., Nie, J.-F., and Qian, M. (2017c). "6 - magnesium alloys," in *Light alloys*. 5th Edn (Boston, MA: Butterworth-Heinemann), 287–367.

Prasad, A., Yuan, L., Lee, P. D., and StJohn, D. H. (2013). The Interdependence model of grain nucleation: a numerical analysis of the Nucleation-Free Zone. *Acta Mater.* 61 (16), 5914–5927. doi:10.1016/j.actamat.2013.06.015

Robson, J. D., and Barnett, M. R. (2019). The effect of precipitates on twinning in magnesium alloys. *Light Mater. Sci. Tech.* 21, 1800460. doi:10.1002/adem.201800460

Robson, J. D., Henry, D. T., and Davis, B. (2009). Particle effects on recrystallization in magnesium–manganese alloys: particle-stimulated nucleation. *Acta Mater.* 57 (9), 2739–2747. doi:10.1016/j.actamat.2009.02.032

Robson, J. D., Stanford, N., and Barnett, M. R. (2010). Effect of particles in promoting twin nucleation in a Mg–5wt.% Zn alloy. *Scripta Mater.* 63 (8), 823–826. doi:10.1016/j.scriptamat.2010.06.026

Sasaki, T. T., Ohkubo, T., and Hono, K. (2009). Precipitation hardenable Mg–Bi–Zn alloys with prismatic plate precipitates. *Scripta Mater.* 61 (1), 72–75. doi:10.1016/j.scriptamat.2009.03.015

Schneider, C. A., Rasband, W. S., and Eliceiri, K. W. (2012). NIH Image to ImageJ: 25 years of image analysis. *Nat. Meth.* 9 (7), 671–675. doi:10.1038/nmeth.2089

Stanford, N., and Barnett, M. R. (2009). Effect of particles on the formation of deformation twins in a magnesium-based alloy. *Mater. Sci. Eng A*. 516 (1), 226–234. doi:10.1016/j.msea.2009.04.001

Stanford, N., and Barnett, M. R. (2013). Solute strengthening of prismatic slip, basal slip and {101¯2} twinning in Mg and Mg–Zn binary alloys. *Int. J. Plast.* 47, 165–181. doi:10.1016/j.ijplas.2013.01.012

StJohn, D. H., Easton, M. A., Qian, M., and Taylor, J. A. (2013). Grain refinement of magnesium alloys: a review of recent research, theoretical developments, and their application. *Metall. Mater. Trans.* 44 (7), 2935–2949. doi:10.1007/s11661-012-1513-x

StJohn, D. H., Prasad, A., Easton, M. A., and Qian, M. (2015). The contribution of constitutional supercooling to nucleation and grain formation. *Metall. Mater. Trans.* 46 (11), 4868–4885. doi:10.1007/s11661-015-2960-y

Sun, Y. H., and Sun, B. Z. (2018). Investigation of structure, morphology and orientation of precipitates in Mg–Bi alloy. *Mater. Char.* 140, 129–133. doi:10.1016/j.matchar.2018.03.042

Suryanarayana, C., and Norton, M. G. (1998). "Crystal structure determination. II: hexagonal structures," in *X-ray diffraction: a practical approach*. (Boston, MA: Springer US), 125–152.

Watanabe, C., Monzen, R., and Tazaki, K. (2008). Effects of Al3Sc particle size and precipitate-free zones on fatigue behavior and dislocation structure of an aged Al–Mg–Sc alloy. *Int. J. Fatig.* 30 (4), 635–641 doi:10.1016/j.ijfatigue.2007.05.010

Yu, H., Fan, S., Meng, S., Choi, J. O., Li, Z., Go, Y., et al. (2020). Microstructural evolution and mechanical properties of binary Mg–xBi (x = 2, 5, and 8 wt%) alloys. *J. Magnesium Alloys* doi:10.1016/j.jma.2020.03.015

Zindal, A., Jain, J., Prasad, R., Singh, S. S., Sarvesha, R., Cizek, P., et al. (2018). Effect of heat treatment variables on the formation of precipitate free zones (PFZs) in Mg-8Al-0.5Zn alloy. *Mater. Char.* 136, 175–182. doi:10.1016/j.matchar.2017.12.018

Conflict of Interest: The authors declare that the research was conducted in the absence of any commercial or financial relationships that could be construed as a potential conflict of interest.